Interval Kalman filtering applied to uninhabited surface vehicle navigation

A Motwani[1], S K Sharma[1], R Sutton[1] and P Culverhouse[2]

[1](School of Marine Science and Engineering, Plymouth University, Plymouth)
[2](School of Computing and Mathematics, Plymouth University, Plymouth)

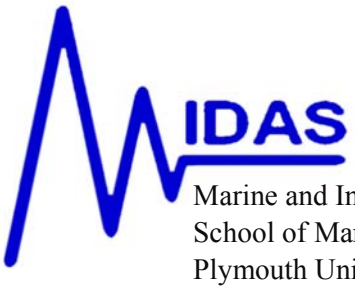

Marine and Industrial Dynamic Analysis
School of Marine Science and Engineering
Plymouth University, PL4 8AA

TECHNICAL REPORT

04 June, 2012

MIDAS.SMSE.2012.TR.003

Abstract

This report discusses the potential application of the interval Kalman filter (IKF) in the design of a navigation system for an uninhabited surface vehicle (USV) named *Springer*. The interval Kalman filter is investigated for this task since it has had limited exposure for such usage. Details of the navigation suite in *Springer* are outlined and a state space model of a TCM2 digital compass which is used to provide simulated heading data is described. In the study, the heading estimation provided by the IKF algorithm developed is compared to that of an ordinary KF, under erroneous system modelling. From the simulated results presented, it is concluded that the IKF has the potential to overcome the shortcomings of the ordinary KF in the face of inaccurate system modelling, albeit the difficulty of its implementation must be dealt with carefully.

1. Introduction

In a review of uninhabited surface vehicles (USVs) (also referred to as unmanned surface vehicles) by Motwani (2012), it can clearly be seen that such craft are now being used in a plethora of marine related applications. For an example, in June 2011, the Ministry of Land, Transport and Maritime Affairs, South Korea, announced a four year USV development programme worth a total of $18.5million (Martin, 2012). Missions envisaged include surveillance, research and monitoring of the oceans. In particular, the vehicle will be used for exclusive economic zone protection duties with a remit for policing illegal fishing and military border intrusions by North Korea.

Irrespective of its allotted task, however, all USVs have two common features. Firstly, such vehicles require robust navigation, guidance and control (NGC) systems in order to cope with possible changes in the dynamic behaviour of a vehicle which may occur owing to the deployment of different payloads, amendments to mission requirements and varying environmental conditions; and secondly, unlike large commercial ships and warships that are equipped with high specification navigational aids such as radio beacons, radar, gyroscopic compasses and inertial measurement units, the navigation suites for USVs are invariably low cost.

As reported by Sharma et al (2012), in recent years at Plymouth University, the *Springer* USV has been designed, built and continues to be developed. The work presented was concerned with the development of a sophisticated autopilot for *Springer*, whereas this paper explores the potential application of interval Kalman filtering (IKF) in the design of a navigation system for the vehicle. The investigation having been instigated as IKF has received minimal attention for application in such roles.

Under normal operating conditions, the *Springer* navigation system employs three low cost digital compasses of differing specifications. However, for this proof of principle study only simulated heading information from a state space of model of one of the digital compasses was utilized. The TCM2 compass being arbitrarily selected for the task.

With regards to the structure and content of the report, following on from this introductory material, section 2 gives details of the navigational sensor suite. Whilst section 3 reports the derivation of a state space model of the TCM2 digital compass used in the sensor suite, and section 4 briefly discusses traditional Kalman filtering. Whereas an introduction to IKFs is given in section 5. Subsequently, results and discussion are then presented in sections 6 and 7 respectively. Finally concluding remarks and an outline of further work are given in section 8.

2. The *Springer* navigation sensor suite.

Since full details of the Springer's hardware have already been recorded in the Journal of Navigation (Sharma et al 2012), only its navigation suite will be considered here. The layout of the Peli cases on board the vehicle that show the location of the sensor suite can be seen in Figure 1. In *Springer*, an integrated sensor suite combines a global positioning system (GPS) receiver, three different types of compasses, speed log and depth sensor. All of these sensors are interfaced to a PC via a NI-PCI 8430/8 (RS232) serial connector. The navigation sensor suite is shown in Figure 2.

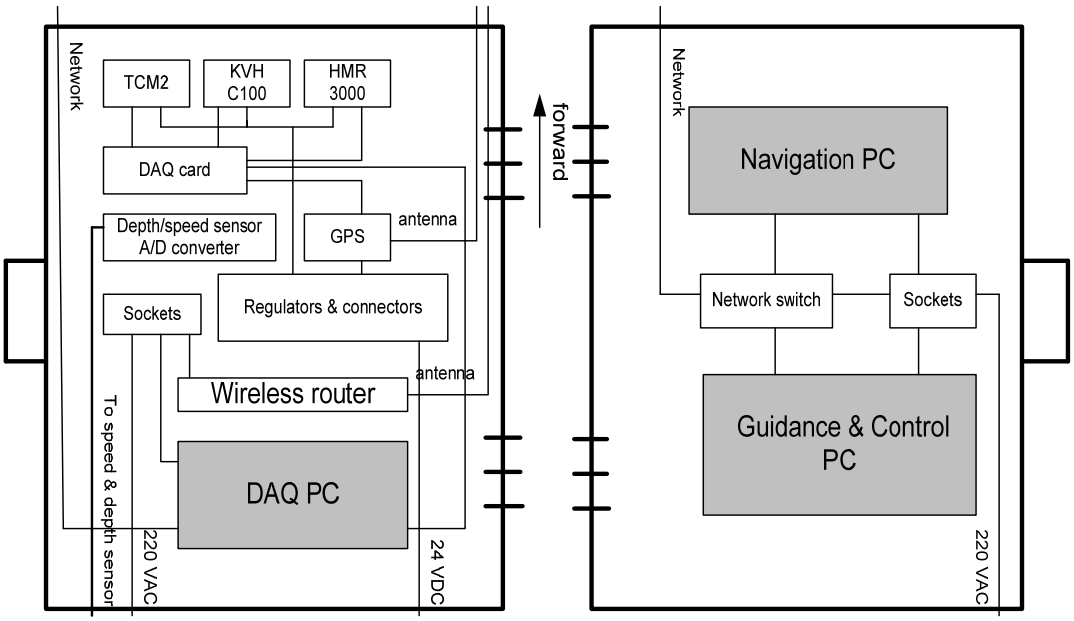

Figure 1, layout of the Peli cases

Since the GPS, depth and speed sensors were not used in this study, their details can be retrieved from elsewhere (Naeem et al 2008). However, although only the TCM2 digital compass is applied herein, details of the three compasses are given in the interest of completeness.

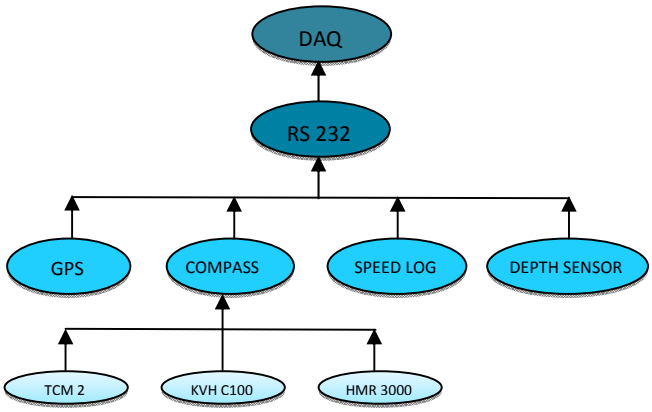

Figure 2, Springer sensor suite.

TCM2, HMR3000 and KVH-C100 are the three different types of electronic compass installed in *Springer*. The TCM2 contains a combined triaxial magneto inductive magnetometer and biaxial fluid filled inclinometer. Unlike traditional technologies, TCM2's magneto-inductive sensor changes inductance due to variances in ambient magnetic field strengths. Thus, power requirements are far below conventional magnetic sensors. It also has a magnetic distortion alarm which is to indicate magnetic anomalies that can compromise compass and inclinometer accuracy.

Whilst, the KVH-C100 is a microprocessor controlled fluxgate compass which consists of a detachable toroidal fluxgate sensor element and a small electronics board. The C100 can accommodate tilt angles up to 450, and has a resolution of 0.10 with an advertised accuracy of 0.50. An innovative automatic compensation algorithm employed in the C100 is largely responsible for the high accuracy obtained by such a low cost system.

Whereas, the Honeywell HMR 3000 digital compass module which includes a magnetic sensor and a liquid filled two-axis tilt sensor is used to provide tilt compensated heading data for *Springer*. It has a high heading accuracy of 0.50 with 0.10 resolution.

All of the compasses can output NMEA 0183 standard sentences with special sentence head and checksum. As all of these compasses are very sensitive, they were mounted as far as possible from any source of magnetic field and from ferrous metal objects as shown in the layout diagram in Figure 1. In addition, each compass was individually housed in a small waterproof case to provided further isolation and insulation. Their specifications are given in Table 1.

Table 1: Specification of each compass

	TCM2	***KVH C100***	***HMR 3000***
Dimension (mm)	73.5x50.8x32.75	114.0x46.0x28.0	74.9x30.5x25.0
Weight (oz)	1.6	14	1
Baudrate	300-38400	300-9600	1200-38400
Supply Voltage (VDc)	+5	+12	+5
Current (mA)	15-20	<40	35
Frequency (Hz)	≤10	≤10	≤10
Temperature (°C)	-20 – 70	-40 – 65	-20 – 70
Tilt range (°)	±50	±80	±40
Output	Digital NMEA 0183	Digital NMEA 0183	Digital NMEA 0183
	Analogue	Analogue	Analogue

3. Compass sensor modelling.

Standard system identification (SI) techniques (Ljung, 1999) were employed to develop the compass sensor model employed here, details of which can be found in Sutton et al (2011). As shown in Equation (1), an Auto-Regressive Moving Average with eXogenous variable (ARMAX) was used for the compass model:

$$A(q^{-1})x(k+n) = B(q^{-1})u(k) + C(q^{-1})e(k) \quad (1)$$

As a result, the TCM2 compass model was obtained:

$$A(q) = 1 - 0.2796q^{-1} - 0.6971q^{-2}$$

$$B(q) = 0.4364q^{-1} - 0.407q^{-2}$$

$$C(q) = 1 + 0.1334q^{-1}$$

The ARMAX model identified above was then simplified into the following as state space model:

$$x_{k+1} = \begin{bmatrix} 0.2796 & 0.6971 \\ 1 & 0 \end{bmatrix} x_k + \begin{bmatrix} 0.4364 & 0 \end{bmatrix}^T u_k + \omega \qquad (2)$$

$$z_k = \begin{bmatrix} 1 & 0 \end{bmatrix} x_k + \upsilon \qquad (3)$$

where ω is the system noise matrix, and the υ the measurement noise matrix,

$$\omega_k \sim N(0, Q_k)$$
$$\upsilon_k \sim N(0, R_k) \qquad (4)$$

Correlation tests having been performed to validate the dynamic characteristics of each of the sensor models.

It should be noted that since the compass had a built in stabilizer filter in order to reduce the cross-coupling effects generated from the pitch and roll axes, these effects were assumed to be small and, as a result, were ignored for simplicity.

4. Kalman Filtering

Since its inception in 1960, the KF (Kalman, 1960) has been used extensively in innumerable applications: although initially used in spacecraft navigation (eg Smith et al, 1961; Schmidt, 1981), it has since been applied in numerous other fields. Tracking problems, such as ballistic missile tracking (Siouris et al, 1997), computer-vision and pattern recognition (eg Ondel et al, 2007), neural network design (Haykin, 2001), change detection systems (Severo and Gama, 2006), manufacturing (Sorenson, 1985), and economics (Bouyé, 2009), illustrate but a few. Also, knowledge of the state-vector is an important aspect of system control (eg Crain, 2002), and the KF is a key part of the optimal linear-quadratic-Gaussian (LQG) control problem (eg, Mäkilä, 2004).

In particular, it has been used extensively for performing sensor data fusion in navigation systems, in which sensor redundancy is favoured when low cost sensors are used and fused to create synergistically a more accurate measurement unit in a probabilistic sense (Xu, 2007).

With such a wide variety of applications, numerous variants of the KF have been developed in an attempt to overcome their shortcomings, such as the extended KF (EKF) (eg, Chui & Chen, 2008) and unscented KF (UKF) (eg, Teixeira et al, 2010).

Basically the KF estimates the true values of the state vector of a dynamic system described by a stochastic-deterministic model, by combining predictions with sensor measurements. The degrees of uncertainty of both the prediction and the measurement are used to compute a weighted average that provides an unbiased estimate of the state vector that minimises the mean square error between it and the true state vector. Although at each measurement update, the KF takes into account all past measurements, the procedure can be made recursive so that data relating to only the previous time-step need be stored, making the KF ideally suited to computer implementation. A detailed description of the algorithm is given in the appendix.

The basic KF scheme yields an optimal estimate only for linear processes with stochastic process and measurement noise that are white and Gaussian, and when these are known precisely along with knowledge of the initial state estimate and estimate error covariance. When the process dynamics are not entirely known and thus not represented correctly, initial estimates are poor, or statistical noise models are inaccurate, the effectiveness of the KF can be compromised. There is no general theory that guarantees a statistically optimal estimate when knowledge of system dynamics and noise statistics are incomplete. Under these situations, it is usual practice to assume some completely specified linear model for the system as well as process and measurement noise covariance matrices. However, this can result in divergence of the predicted mean square state estimation error that typically remains bounded from the actual mean square error which may diverge (Price, 1968).

5. Interval Kalman filtering.

In practice, process dynamics are only known with some degree of certainty. The basic approach to handling this inconvenience has traditionally been to appeal to a probabilistic description of this uncertainty via the inclusion of a process and a measurement noise, and apply a statistically optimal filter such as the KF. This approach carries with it the necessity to introduce experimentally some distribution law describing the process and measurement noise (first and second order moments, if Gaussian noise is assumed, as is the case of the KF) (Kolev, 1993).

An alternative approach to treating processes with uncertain data is to apply the notion and methods of interval analysis. The idea of using interval arithmetic to describe the uncertainty in the system model has been proposed. With such a description, IKF equations (Figure 3) have been obtained using the same derivation as the regular KF but applied to an interval system (Chui & Chen, 2008). Suppose some elements of the matrices A, Γ, and C are uncertain within some definite bounds. The process can then be described as:

$$\begin{cases} x_{k+1} = A_k^I x_k + B_k^I u_k + \Gamma_k^I \xi_k \\ z_k = H_k^I x_k + \eta_k \end{cases} \tag{5}$$

where $M_k^I = M_k \pm \Delta M_k = [M_k - |\Delta M_k|,\ M_k + |\Delta M_k|]$ for $M \in \{A, B, \Gamma, H\}$, and ξ_k and η_k are white noise sequences with zero mean Gaussian distributions with known (or assumed) covariances $var(\xi_k) = Q_k$ and $var(\eta_k) = R_k$, and that $E(\xi_l \eta_k^T) = 0\ \forall l, k$, $E(x_0 \xi_k^T) = 0$ and $E(x_0 \eta_k^T) = 0\ \forall k$.

The IKF algorithm yields the state estimate as an interval vector $\hat{x}_k^I$ for each time step k (Figure 4), and can be summarised by the following equations, which mimic those of the ordinary KF but are described in terms of intervals (Figure 3) (Chui & Chen, 2008).

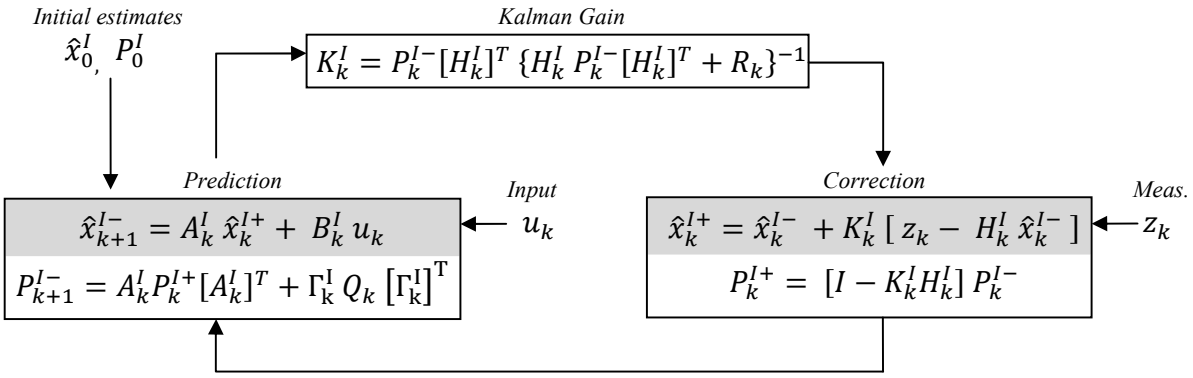

Figure 3: IKF recursive formulation

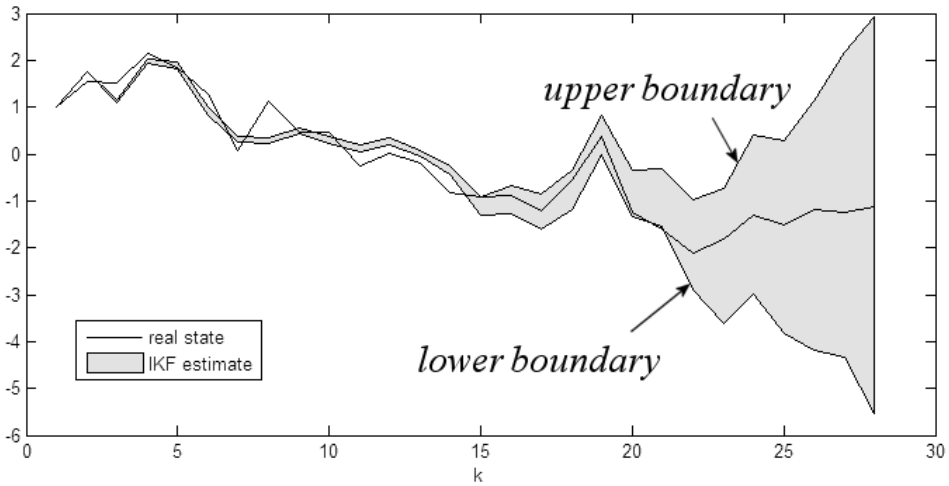

Figure 4: IKF estimate depicting its upper and lower boundaries

Having been derived upon the same principles, the IKF is statistically optimal in the same sense as the standard KF, and it maintains the same recursive formulation. However, the result of the IKF is a sequence of interval estimates rather than point estimates, the fundamental advantage of which being that this guarantees infallible bounds on the true value of the estimate. Also, using machine interval arithmetic means that computer round-off errors are automatically accounted for when implemented on computers (Kolev, 1993).

One of the difficulties of implementing the IKF lies in the computation of the inverse interval matrix for the Kalman gain. Singularity problems arise when there are intervals containing zero. In the field of interval mathematics, the problem of inverting interval matrices has been given less attention than that of solving systems of linear interval equations. Owing to this, several workaround strategies to by-pass these difficulties have been proposed. For instance, Chen et al (1997) proposed a "suboptimal IKF" in which the inverse interval matrix is replaced by its worst-case inversion, which is an ordinary (non-interval) matrix.

Another practical difficulty encountered in the implementation of the IKF is that the interval estimate trajectory diverges due to the conservative nature of interval modelling. The range of interval values is often excessively wide due to the inclusion of all possible estimates produced by the interval system. The rapid expansion of the boundaries makes the IKF unsuitable to be implemented on a computer as the digital representation limits would soon be surpassed.

A few theoretical proposals have been put forward towards resolving this difficulty. Chui and Chen (2008) have proposed a weighted-average IKF to obtain a point-value estimate from the interval estimate. However, the problem of selecting which point-estimates to compute an average from, their relative weights, and how this affects the estimated error covariance (which is also obtained as interval estimates) remains to be researched.

In this simulation study, the IKF is applied to determine the heading of the *Springer* vehicle using the TCM2 compass model described earlier. The approach suggested by Chui & Chen to avoid divergence of the IKF will be used – in the absence of any weighting criteria, a simple averaging of the boundaries will be conducted. A comparison is then made between the estimates provided by an ordinary KF and the IKF under erroneous model assumptions, and conclusions thence drawn.

It is to be noted that the IKF has been implemented with the aid of INTerval LABoratory (INTLAB), an interval arithmetic toolbox for MATLAB developed by Prof Rump at Hamburg University (Rump, 1999).

6. Simulation and results.

For this study, it is assumed that the compass model given by equations (2) and (3) is not completely accurate. For simplicity, the discrepancy between model and actual dynamics is made to lie solely within the first term of the dynamic matrix, so that the true value is 2 percent over the modelled value. That is,

$$x_{k+1} = Ax_k + Bu_k + \xi_k \qquad (6)$$
$$z_k = H\,x_k + \eta_k$$

represents the actual compass dynamics, and

$$x_{k+1} = A_m x_k + B_m u_k + \xi_k \qquad (7)$$
$$z_k = H_m\,x_k + \eta_k$$

the modelled dynamics, where

$$A_{11} = 1.02\,A_{m,11} \text{ and } A_{ij} = A_{m,ij}\,,(i,j\text{-}) \neq (1,1)$$
$$B = B_m,\ H = H_m$$
$$A_m = \begin{bmatrix} 0.2796 & 0.6971 \\ 1 & 0 \end{bmatrix},\ B_m = \begin{bmatrix} 0.4364 \\ 0 \end{bmatrix},\ C_m = [1,0],\ D_m = 0 \qquad (8)$$
$$Q = \begin{bmatrix} 1 & 0 \\ 0 & 1 \end{bmatrix},\qquad R = 4;$$
$$E\{\xi_k \xi_l^T\} = \delta_{kl}\,Q\ ;\ E\{\eta_k \eta_l^T\} = \delta_{kl} R;\ E\{\xi_k \eta_l^T\} = 0;$$

with both ξ_k and η_k being normally distributed. Note that the values obtained for the compass state space model obtained in section 3 are the ones replicated in (8). If one assumes that the compass output is proportional to its heading angle, then the (erroneous) model introduces a steady-state bias to the measurement that is proportional to the internal state.

Figure 5 shows the idealised scaled output of the compass to a changing in its heading angle, that is, the output if there were no random perturbations. This changing angle is the one that is used as input to the state-space equations in all the subsequent simulations.

Figure 6 depicts a simulation of the first component of the real compass state according to (6) (including noise processes). Henceforth, simulation will be shown only for the first component of the state vector, though the discussion is valid for the complete state vector, as similar results were obtained for the second component. Figure 6 also portrays the KF estimate of the state. The KF equations used are given in the appendix, for which the model (7) was used. The divergence of the KF estimate from the actual state is evidenced, and it is due to the incorrect modelling of the system dynamics.

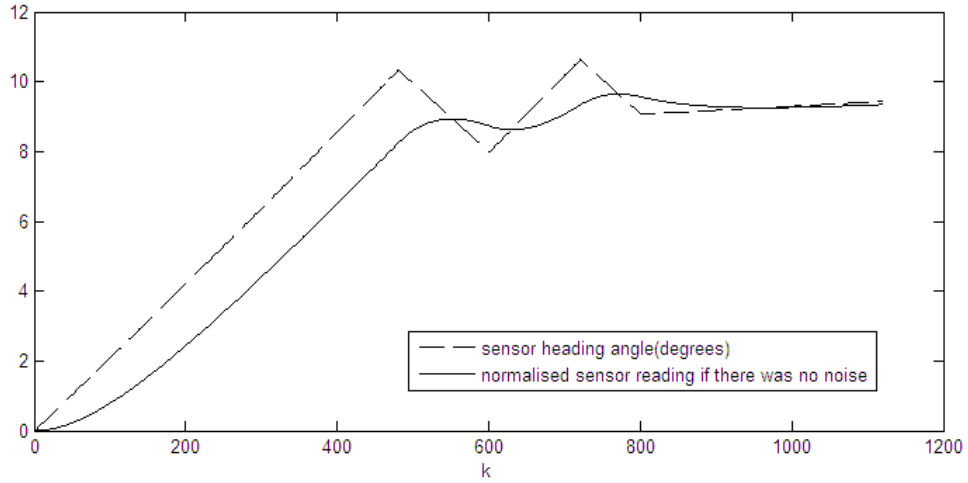

Figure 5, showing the response of the compass to an evolving heading angle, where the response has been scaled to match the input.

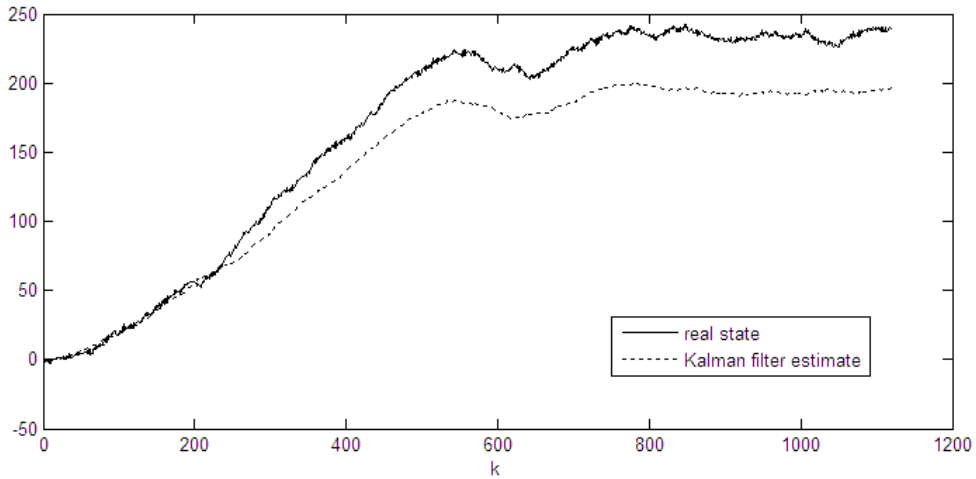

Figure 6, comparison of true state estimate and KF estimate: the KF estimate diverges from the true state because of the incorrect system model used in the filter equations.

In an attempt to tackle this divergence and IKF is implemented based on the following model, in which the first term of the interval dynamic matrix contains a parametric uncertainty that encompasses the modelling error.

$$x_{k+1} = \begin{bmatrix} [0.8 \times 0.2796,\ 1.2 \times 0.2796] & 0.6971 \\ 1 & 0 \end{bmatrix} x_k + B_m u_k + \xi_k \qquad (9)$$

$$z_k = H_m\, x_k + \eta_k$$

The implementation of the IKF through the recursive use of the equations shown in Fig 3 alone is not practical due to the conservative nature of the interval computations *per se*: the evaluation of expressions in interval arithmetic leads to typically larger intervals in the results, as these have to contain all possible values of the operands, combining these in all possible ways. In fact, raw implementation of the IKF recursive algorithm results in rapidly expanding intervals, the boundaries surpassing maximum floating point ranges very quickly. To avoid this, some mechanism to limit the growth of the intervals must be incorporated into the algorithm.

The first strategy used here consists simply of resetting the interval estimates to their mid-point values, for both the state vector and error covariance estimates, when the interval ranges approach intractable values. Specifically, at each time-step the new state and error covariance estimates are computed from the previous ones, and their finiteness is tested. If the test fails, then these estimates are discarded, and the IKF estimates are recalculated instead from the mid-range values of the previous state and error covariance estimates (it is to be noted that the concept of finiteness herein refers to being within the range of representable floating point reals – eg, for the IEEE 754 double precision floating point format, approximately from 2.22e-308 to 1.79e308). Although this in principle would allow the continual application of the algorithm, to avoid extremely large interval ranges for the state estimate, a further criterion is adopted whereby the same 'reset' procedure is carried out if the resulting interval estimate obtained from the application of the IKF, while being finite, is larger than a predefined threshold. Figure 7 depicts the upper and lower IKF state estimate boundaries obtained when the threshold was set to 50, as well as the true state and ordinary KF state estimate. The mid-values of the intervals obtained by averaging the boundaries is shown in Figure 8.

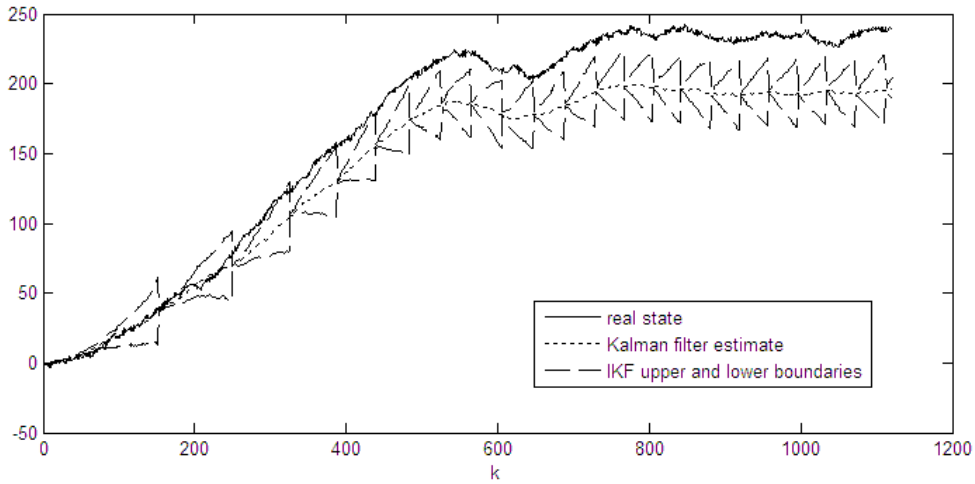

Figure 7, IFK boundaries using reset mechanism with a threshold value of 50, shown together with true state evolution and ordinary KF estimate.

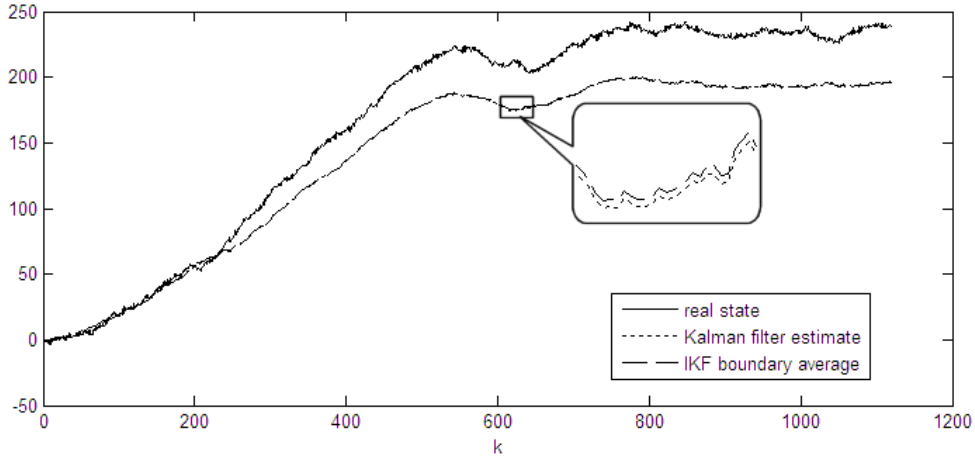

Figure 8, mid-values of the IFK intervals shown in figure 7, along with true state evolution and ordinary KF estimate.

As can be seen from figures 7 and 8, the IKF estimate practically follows the regular KF estimate, though it is to be noted from figure 8 that the average IKF estimate is ever so slightly closer to the true state than the regular KF estimate. The same IKF estimation strategy was applied increasing the threshold value by tenfold, to 500. The corresponding results are shown in figures 9 and 10.

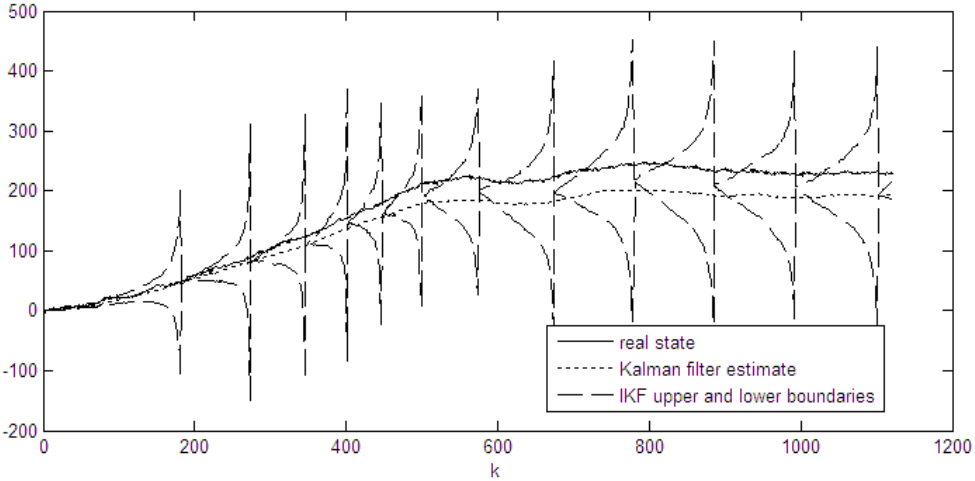

Figure 9, IFK boundaries using reset mechanism with a threshold value of 500, shown together with true state evolution and ordinary KF estimate.

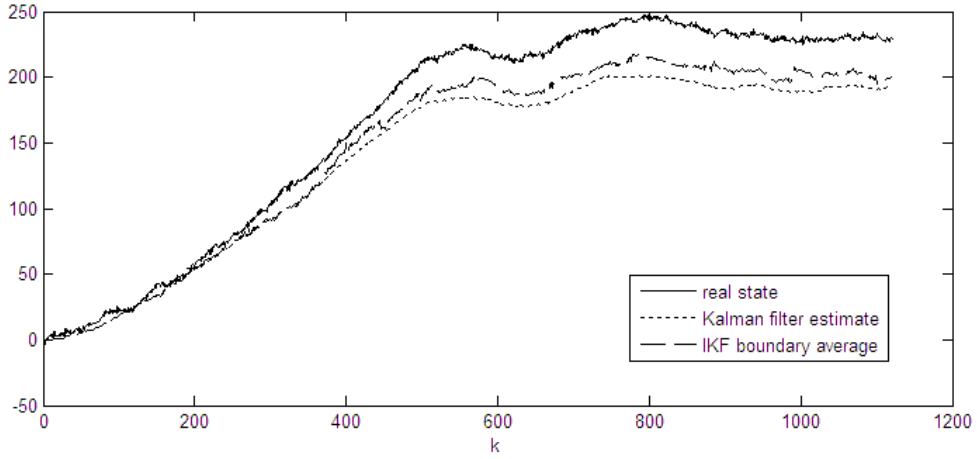

Figure 10, mid-values of the IFK intervals shown in figure 9, along with true state evolution and ordinary KF estimate.

The effect of raising the threshold is seen in figures 9 and 10. The average IKF estimate, while still biased with respect to the real state, is less so than with the smaller threshold value, and is a clear improvement over the estimate of the ordinary KF. This self-correcting trend continues with a further increase of the threshold, albeit with a price. Upon increasing the threshold value by another factor of 10, the upper and lower boundaries of the IKF are allowed to take on take on values well outside the scale of the preceding figures. However, the average value of the boundaries is shown in figure 11.

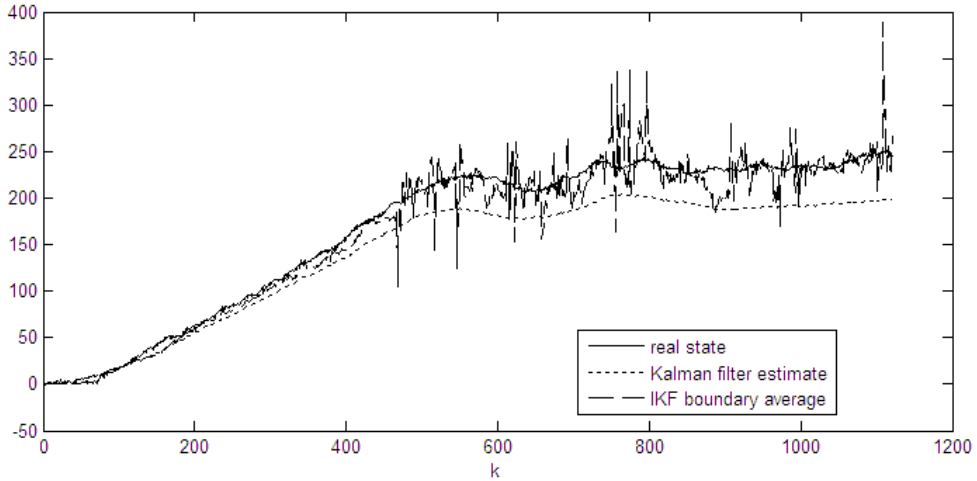

Figure 11, mid-values of the IFK intervals using reset mechanism with a threshold value of 5000, shown together with true state evolution and ordinary KF estimate.

Two things are gleaned from figure 11: on the one hand, the average IKF estimate now follows the real state, but on the other, it does so with volatile oscillations between time steps. Further increases of the threshold allow further heightening of the size of the intervals, but in terms of the mid-range estimation curve no significant differences are observed.

Before discussing these phenomena, a second strategy is implemented for the IKF. Like in the previous case, the IKF state and error covariance estimates are tested for finiteness, and in the case of the state interval, compared against a threshold value. When the test is negative though, instead of drastically reducing the intervals to point values at their centres, a pre-specified percentage reduction is applied that narrows the intervals down by conserving only that percentage of each interval symmetrically with respect to its centre. If however this reduction is insufficient to yield a successive estimate that passes the finite and threshold tests, it is re-applied recursively until the test is passed. The result of applying this procedure with a threshold of 50 and a reduction parameter of 50% is shown in figure 12.

It can be observed in figure 12 how this method manages to keep a relatively uniform boundary width of the IKF state estimate. However, the boundaries are centred around the erroneous ordinary KF estimate, rather than the true state. The effects of applying an even more gradual reduction of the interval widths is shown in figure 13, for which the reduction parameter was changed from 50% to 90%. Figure 14 shows the average of the IKF boundaries of figure 13.

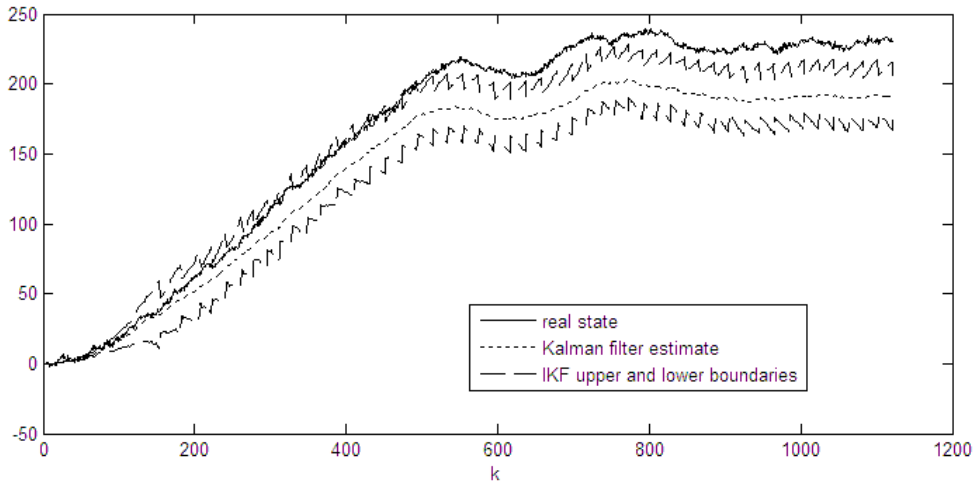

Figure 12, boundaries of the IFK intervals using percentage reduction mechanism with a threshold value of 50 and reduction parameter of 50%, shown together with true state evolution and ordinary KF estimate.

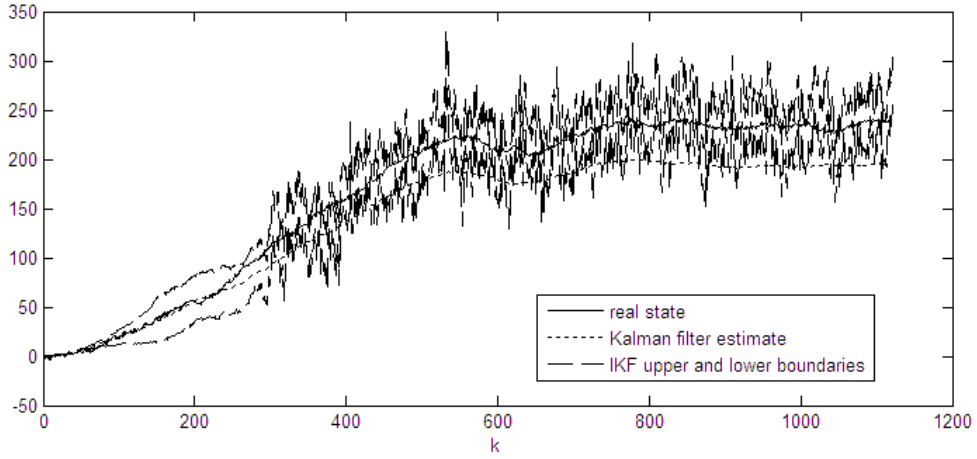

Figure 13, boundaries of the IFK intervals using percentage reduction mechanism with a threshold value of 50 and reduction parameter of 90%, shown together with true state evolution and ordinary KF estimate.

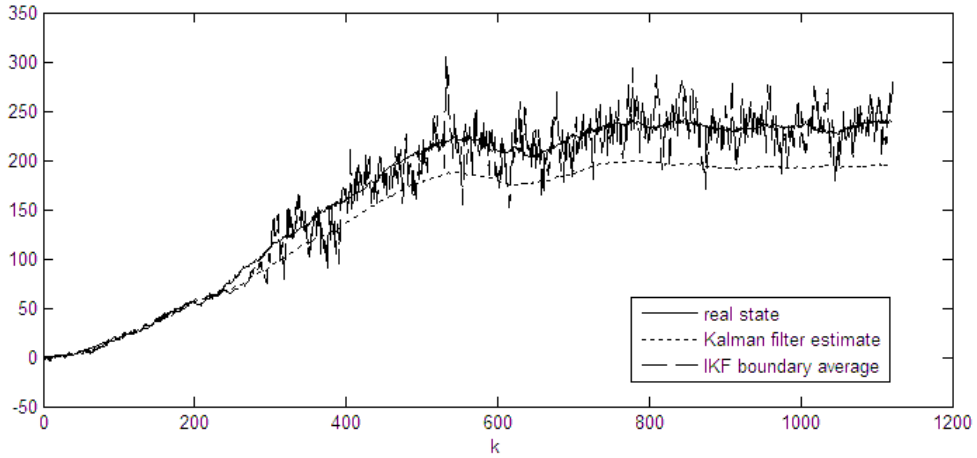

Figure 14, mid-values of the IFK intervals using percentage reduction mechanism with a threshold value of 50 and reduction parameter of 90%, shown together with true state evolution and ordinary KF estimate.

.

Although the boundaries seem more haphazard, it can now be seen that they are centred around the true state rather than the erroneous KF estimate. This is confirmed in figure 14. Admittedly the mid-value estimate contains relatively volatile oscillations, however, the application of an averaging filter shows that on average the estimate closely follows the true state, as is shown in figure 15. (It is to be noted that this averaging filter has been applied *a posteriori* by averaging each value with its closest10 neighbours on either side, hence this filter cannot be applied on the fly, at least not without a delay. Also, the strong oscillations at the end simply correspond to the unfiltered tail-enders).

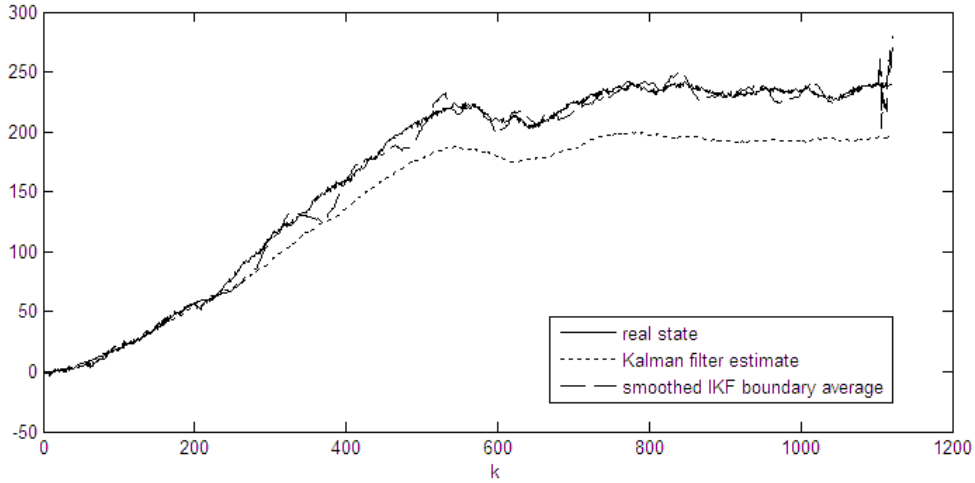

Figure 15, smoothed version of the mid-values of the IFK estimate of figure 14, shown together with true state evolution and ordinary KF estimate.

Finally, figure 16 shows the effect of reducing the threshold from a value of 50 to 25. As can be observed, the IKF boundaries, though comparatively smooth, have shifted from being centred around the true state to the erroneous ordinary KF state estimate.

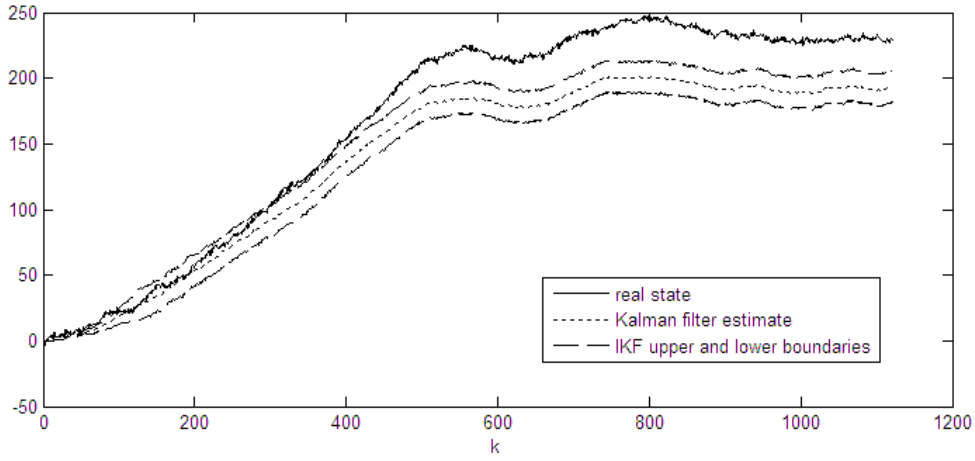

Figure 16, boundaries of the IFK intervals using percentage reduction mechanism with a threshold value of 25 and reduction parameter of 90%, shown together with true state evolution and ordinary KF estimate.

7. Discussion

The simulations of the previous section evidence an important aspect of the nature of the IKF. While the raw IKF algorithm cannot be applied for more than a few time steps at a time, the two strategies described here are designed to allow one to effectively apply the IKF for as long as possible before computer restraints force the IKF intervals to be artificially curbed. The additional threshold parameter allows one to explore the effect of bringing in this subduing mechanism earlier or later, within the computer limitations.

Basically, the severity of the artificial suppression dictates the outcome. When the intervals are not allowed to grow enough (eg, by using a threshold value of 50 with the centre-value reset mechanism, figure 7), the IKF basically gives the same estimates as the ordinary KF (in an averaged sense). However, loosen this restriction, and the IKF starts homing in on the true state estimate where there ordinary KF cannot (figures 9-11), even though no extra information to adapt the filter model has been used: the IKF adapts its course according to the true measurements. This evidences an important fact of the IKF: the IKF has the inherent capability of correctly estimating the system state even when the system model is not known precisely but is known within finite bounds. This means that the IKF is robust to bounded uncertainty in the system state space parameters, unlike the ordinary KF. However, the imperious caveats to this impressive statement have been shown in the previous simulations and their severity is not to be underestimated. The inherent robustness of the IKF is only feasible if the IKF were allowed to function unhindered by physical limitations (absolute maximum real values that can be represented on a computer), and this is obviously far from possible. The IKF intervals grow in an unbounded fashion, and do so relatively quickly. Thus the exploitation of its inherent virtue to overcome erroneous estimation in the face of modelling uncertainty is limited by these physical limitations.

The two mechanisms to fetter the growth of the IKF intervals presented here are not in themselves robust solutions to the problem of practical implementation of the IKF. As can be seen from the simulations, the effectiveness of the IKF is very sensitive to the choice of restricting parameters. While the application of the progressive percentage reduction of the intervals allows the IKF more manoeuvrability to adapt its course the centre-value reduction scheme, both using the same reset value threshold than, the choice of these parameters is a problem on its own. Not only that, increased manoeuvrability for the IKF results in estimates that, although unbiased, tend to have non-smooth characteristics.

The mechanisms used here to try and simulate the longer-term IKF behaviour succeed to a certain extent, but use no criteria to favour the IKF estimate themselves (in fact, they are in every way restrictive distortions imposed that simply allow the continuous application of the IKF algorithm). However, they have allowed the IKF's virtues to be exposed, with all the more merit to the IKF itself. They also constitute simple and practical ways of allowing the IKF to be implemented and are shown to be able to overcome the bias of the ordinary KF estimate, with the right choice of parameters, when simulated with the compass system. Thus, one possibility is to employ them simply to correct this bias of the ordinary KF estimate.

8. Concluding remarks and future work.

The IKF yields conservative estimates as it contains all the optimal (in the same sense as the KF) estimates of all the point-value systems included in the interval system. But because of this, the intervals become intractably large very early on in the simulation, exceeding computer representation limits. The present study uses artificial mechanisms to allow prolonged simulation of the IKF. Albeit these mechanisms are interferential, under the right circumstances they do allow the virtues of the IKF to be exposed, namely, its inherent robustness in the face of bounded modelling errors.

This raises the following challenge: to find artificial mechanisms that allow prolonged operation of the IKF without distorting it, or if possible, even assisting it to direct itself towards the true state estimates. Some attempts at using AI techniques have already been suggested (Weng et al 2000), and it is thought that work should continue towards this goal to provide practical and feasible solutions that can be implemented in real time.

Appendix

Basically, the KF is an estimator. The need for such an estimator arises when it is necessary to appraise the value of some quantity that cannot be measured without some degree of uncertainty. In nature, all processes contain some degree of noise or disturbance that cannot be accounted for in a deterministic fashion, and this includes measuring devices. For example, micro electro-mechanical accelerometers are subject to electronic noise from ambient electromagnetic fields that bear upon the circuitry that converts motion into a voltage signal, as well as mechanical noise, such as thermo-mechanical noise that results from molecular agitation which affects the small moving parts of the sensor (Mohd-Yasin et al, 2010).

Not only do all processes have inherent noise, but also, process models only describe real processes with a certain degree of accuracy. Real processes may also be affected by unmeasurable external disturbances that are not accounted for: for example, the velocity of a vehicle is perturbed by gusts of wind that cannot be foreseen as deterministic inputs to the velocity model of the vehicle.

To account for these uncertainties, stochastic descriptions of processes must be used. The Kalman filter was originally designed to estimate the state vector of a system described by the following linear deterministic-stochastic process:

$$\begin{cases} x_{k+1} = A_k x_k + B_k u_k + \Gamma_k \xi_k \\ z_k = H_k x_k + \eta_k \end{cases} \tag{10}$$

where x_k, u_k, and v_k are, respectively, the state vector, the (deterministic) process input, and the measurement vector at time-step k, and ξ_k and η_k are the process noise and measurement noise sequences, which account for the uncertainty in the process and measurements respectively.

If it is assumed that ξ_k and η_k are white noise sequences with zero mean Gaussian distributions with known (or assumed) covariances $var(\xi_k) = Q_k$ and $var(\eta_k) = R_k$, and that $E(\xi_l \eta_k^T) = 0 \; \forall l, k$, $E(x_0 \xi_k^T) = 0$ and $E(x_0 \eta_k^T) = 0 \; \forall k$, then the KF equations provide a statistically optimal estimate of the state vector, and can be written as a set of recursive equations (figure 17) (see, for example, Chui & Chen, 2008).

The KF equations allow one to recursively obtain the state estimate at each time step from the previous estimate and new observed data, assuming initial estimates for x_0 and P_0. The advantage of the recursive formulation is that only the previous estimate needs to be stored, as the necessary information of all previous data is contained in it, which makes the computation at each time step feasible. Under the stated hypothesis, the KF provides an unbiased and minimum error variance estimate of the process state vector.

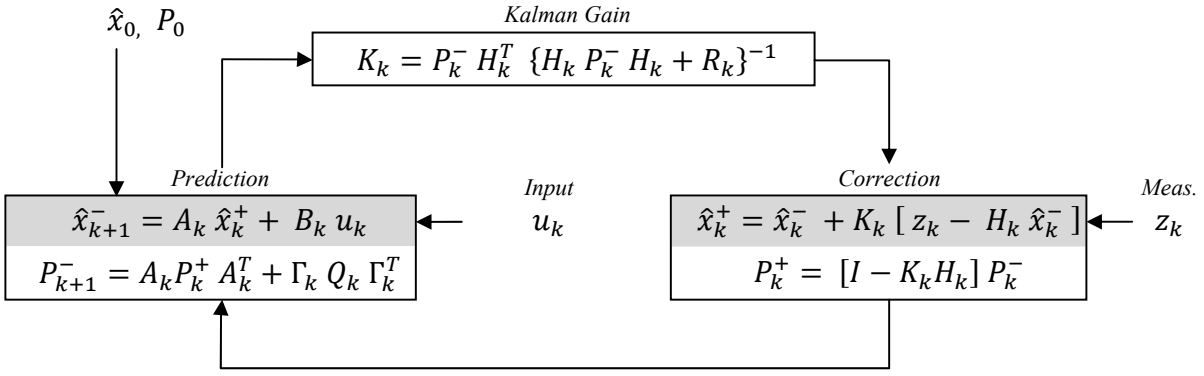

Figure 17: Kalman filter recursive formulation

References

Bouyé, E.(2009), *Kalman Filter: some applications to Finance*. Financial Econometrics lectures notes, University of Evry.

Chen, G., Wang, J. and Shieh, L. S. (1997). *Interval Kalman Filtering*. IEEE Transactions on Aerospace and Electronic Systems 33(1), pp.250–258.

Chui, C.K. & Guanrong Chen, G. (2008). *Kalman filtering with real-time applications*. 3rd edition, Springer-Verlag Berlin Heidelberg.

Crain T. P. (2002). *Kalman Filters as Dynamic System State Observers*. Mechatronics Handbook, CRC Press LLC.

Haykin S. (2001). *Kalman Filtering and Neural Networks*. Volume 23 of Adaptive and learning systems for signal processing, communications, and control, John Wiley & Sons.

Kalman, R. E. (1960). *A New Approach to Linear Filtering and Prediction Problems*. Transactions of the ASME, Journal of Basic Engineering, 82, Series D (March), pp 35-45.

Kolev L. (1993). *Interval Methods for Circuit Analysis (Advanced Series in Circuits & Systems)*, World Scientific Publishing Co Ltd, Singapore.

Ljung, L. (1999). *System Identification: Theory for the User*. 2nd ed., Prentice Hall Inc, New Jersey.

Mäkilä P.M. (2004). *Kalman Filtering and Linear Quadratic Gaussian Control*, Lecture notes for course 7604120, Institute of Automation and Control, Tampere University of Technology, Tampere, Finland.

Martin, A. (2012). New Wave. *Unmanned Vehicles*, Vol 16, No 6, January, pp.15-18.

Mohd-Yasin, F., Nagel, D. J. and Korman, C. E. (2010). *Noise in MEMS*. Measurement Science and Technology 21(1), 012001.

Motwani, A. (2012). *A Survey of Uninhabited Surface Vehicles*. MIDAS Technical Report: MIDAS.SMSE.2012.TR.001, Plymouth University. Available at: www.springer-usv.com

Naeem W, Xu T, Sutton R and Tiano A (2008). *The Design of a Navigation, Guidance, and Control System for an Unmanned Surface Vehicle for Environmental Monitoring*. Proc Instn Mech Engrs Part M: Journal of Engineering for the Maritime Environment, Vol 222, No M2, pp.,67-80.

Ondel O., Boutleux E., Clerc G., Blanco E. (2007). *FDI based on pattern recognition using Kalman prediction: Application to an induction machine*, Engineering Applications of Artificial Intelligence, 21(7), pp 961-973.

Price, C.F. (1968). *An analysis of the divergence problem in the Kalman filter*. IEEE Transactions on Automatic Control, 13(6), pp 699-702.

Rump, S. (1999). *INTLAB - INTerval LABoratory*. Kluwer Academic Publishers.

Schmidt, S. F. (1981). *The Kalman Filter: Its Recognition and Development for Aerospace Applications*. Journal of Guidance and Control, 4(1), pp 4-7.

Severo M., & Gama J. (2006). *Change Detection with Kalman Filter and CUSUM*, Proceedings of Discovery Science, 7-10 October, Barcelona, Spain, pp.243-254.

Sharma S.K., Naeem W., & Sutton R. (2012). *An Autopilot Based on a Local Control Network Design for an Unmanned Surface Vehicle*. Journal of Navigation, 65, Issue 2, pp.281-301.

Siouris G.M., Chen G. and Wang J. (1997), *Tracking an incoming ballistic missile using an extended interval Kalman filter*. IEEE Transactions on Aerospace and Electronic System, 33(1), pp 232-239.

Smith, G. A., Schmidt, S. F., & McGee, L. A. (1961). *Application of statistical filter theory to the optimal estimation of position and velocity on board a circumlunar vehicle.* Technical Report R-35. Moffett Federal Airfield, CA.

Sorenson, H. W. (1985), *Kalman Filtering: Theory and Application*, (ed) IEEE Press, New York, 1985.

Sutton R, Sharma S and Xu T (2011). *Adaptive Navigation Systems for an Unmanned Surface Vehicle.* Proc IMarEST - Part A: Journal of Marine Engineering and Technology, Vol.10, No 3, Sept, pp. 3-20.

Teixeira B.O.S, Torres L.A.B, Aquirre L.A. & Bernstein D.S. (2010). *On Unscented Kalman Filtering with State Interval Constraints*. Journal of Process Control, Vol 20, No 1, pp. 45-57.

Weng, Z., Chen, G., Shieh, L. S. and Larsson, J. (2000). *Evolutionary programming Kalman filter.* Information Sciences 129(1-4), pp.197–210.

Xu, T. (2007). *An intelligent navigation system for an unmanned surface vehicle.* PhD thesis, Plymouth University.

Nomenclature / List of Acronyms

EKF	Extended Kalman Filter
GPS	Global Positioning System
IKF	Interval Kalman Filter
KF	Kalman Filter
NGC	Navigation, Guidance, and Control
UKF	Unscented Kalman Filter
USV	Uninhabited Surface Vehicle / Unmanned Surface Vessel
Q	Process Noise Covariance
R	Measurement Noise Covariance